Applied Surface Science 462 (2018) 453–465

Contents lists available at ScienceDirect

Applied Surface Science

journal homepage: www.elsevier.com/locate/apsusc

Full Length Article

Rational design of magnetic infinite coordination polymer core-shell nanoparticles as recyclable adsorbents for selective removal of anionic dyes from colored wastewater

Wei Huang[a], Junzhe Xu[a], Dingkun Lu[a], Jingjing Deng[a,b,*], Guoyue Shi[c], Tianshu Zhou[a,b,*]

[a] School of Ecological and Environmental Sciences, Shanghai Key Lab for Urban Ecological Process and Eco-Restoration, East China Normal University, 500 Dongchuan Road, Shanghai 200241, China
[b] Institute of Eco-Chongming, 3663 Zhongshan Road, Shanghai 200062, China
[c] Department of Chemistry, East China Normal University, 500 Dongchuan Road, Shanghai 200241, China

ARTICLE INFO

Keywords:
Fe_3O_4@Tb/AMP core-shell nanoparticles
Recyclable adsorbents
Anionic dyes
Selective adsorption
Magnetic separation
Colored wastewater

ABSTRACT

In this study, novel magnetic infinite coordination polymer Fe_3O_4@Tb/AMP core-shell nanoparticles were rationally designed and fabricated as recyclable adsorbents for selective removal of anionic dyes from colored wastewater. The core-shell nanoparticles used in this study are composed of two components: the shell is the supramolecular infinite coordination polymers (ICPs) network formed by terbium ions (Tb^{3+}) and adenosine 5′-monophosphate monohydrate (AMP) ligands and the core is the Fe_3O_4 nanoparticles which are encapsulated into the ICP network by the self-adaptive inclusion process. The prepared core-shell nanoparticles showed superiority in strong magnetism and selective adsorption towards anionic dyes, such as Alizarin Red (AR) and Congo Red (CR). Parameters that influenced the adsorption process, such as solution pH, salt concentration and adsorbent dosage were investigated. Under the optimal conditions, adsorption kinetics, isotherms and thermodynamics were also determined. Notably, this nano-adsorbent exhibited rapid adsorption feature (almost 96% dye removal in 5 min) and the adsorption isotherm data fitted quite well with the Langmuir model with an estimated maximum adsorption capacity of 357.14 mg g^{-1} for AR and 909.09 mg g^{-1} for CR at 298 K. This capacity could be further enhanced at the higher temperatures. In addition, the Fe_3O_4@Tb/AMP core-shell nanoparticles could be regenerated by a simple salt/ethanol-washing method and used with high recyclability over five cycles. With the magnetically separable Fe_3O_4@Tb/AMP core-shell nanoparticles as adsorbents, selective removal of toxic anionic dyes from colored wastewater could be realized directly, which is of great importance for the sustainable development of dye contaminated wastewater treatment technology.

1. Introduction

With the fast development of social economy and rapid pace of industrialization, environmental pollution, in particular dye wastewater pollution, has become one of the serious issues. Over the past few years, the synthetic dyes are widely used in textiles, plastics, rubber, cosmetics, printing, leather, pharmaceuticals and food processing industries [1–3]. Based on the different chemical structures, the dye molecules can be classified as anionic (direct, acid, reactive), cationic (basic) and nonionic (disperse). Among these, reactive dyes are extensively used, for example, azo and anthraquinone, two major classes of reactive dyes, together represent 90% of all organic colorants. Due to their interaction with hydroxyl ions in the solution, these dyes are always wasted in the dyeing process, remained in the effluents and are hardly eliminated under aerobic conditions [4–6]. The inappropriate disposal of wastewater containing these dyes to the aquatic ecosystems directly causes great harm to public health and ecological equilibrium [7]. In the provision of clean water, it is imperious to realize efficient removal of dyes from wastewater [8–10]. Chemical and biological methods are very effective for the treatment of dye wastewater, but the requirements of large amounts of supporting materials and generation of by-products limit their applications, especially for those anionic dyes with high water solubility and low biodegradability. In comparison, owing to the simplicity, low cost and high efficiency, removing dyes through physical adsorption is deemed as an adaptable method [11–13]. However, it is not an easy task to take care of the effluents

* Corresponding authors at: School of Ecological and Environmental Sciences, Shanghai Key Lab for Urban Ecological Process and Eco-Restoration, East China Normal University, 500 Dongchuan Road, Shanghai 200241, China.
E-mail addresses: jjdeng@des.ecnu.edu.cn (J. Deng), tszhou@des.ecnu.edu.cn (T. Zhou).

https://doi.org/10.1016/j.apsusc.2018.08.122
Received 7 May 2018; Received in revised form 19 July 2018; Accepted 16 August 2018
Available online 18 August 2018
0169-4332/

containing anionic dyes for probable industrial reuse. Recyclable adsorbents with tailorable selectivity to isolate anionic dye species in colored wastewater is a great challenge.

So far, a variety of nanostructured porous materials are preferred in adsorption technology due to the smaller size, higher surface area and inter particle interaction affinity, for example, carbon-based materials, metal-organic frameworks (MOFs) or zeolitic imidazole frameworks (ZIFs) have been widely used for dye adsorption with the improved effectiveness and efficiency [14–20]. Recently, nanoscale infinite coordination polymer (ICP) particles have stimulated our interest. Unlike their counterparts of MOFs or ZIFs, ICPs are amorphous nanoparticles of supramolecular coordination polymer networks self-assembled from metal ions and multitopic ligands in a mild condition. They typically lack crystallinity and therefore a well-defined framework. While this "structural flexibility" can certainly be a disadvantage in certain applications, it is of key importance to fabricate the recyclable adsorbents for selective removal of particular dyes, because of the following reasons: (1) highly tailorable metal ions and ligands allowed for recognizing dyes through some specific binding, such as the ionic interactions, hydrogen bonding, p-p interactions [21,22]; (2) adjustable porosities and structural flexibility could be rationally tuned to accommodate dyes by adapting to the shape of guest molecules [23]; (3) and most importantly, excellent adaptive capability of guest encapsulation facilitated the formation of novel adsorbents with multifunctionalities through simple "one-pot" reaction [24–29]. The as-formed ICP adsorbents combine the inherent properties of porous network and functional guest (i.e., magnetic nanoparticles), which could be favorable to realize fast and convenient separation in the processing and recovery stages and is more adaptive for selective removal of anionic dyes from colored wastewater.

In this study, we for the first time reported the magnetic infinite coordination polymer Fe_3O_4@Tb/AMP core-shell nanoparticles as recyclable adsorbents for selective removal of anionic dyes, Alizarin Red (AR, anthraquinone) [30], Congo Red (CR, azo) [31] as model, from colored wastewater by taking the advantage of their host-guest synergetic effect. Herein, positive trivalent lanthanide ions Tb^{3+} with large coordination numbers, versatile coordination geometry and high coordination flexibility were selected as central metal ion, nucleotides 5′-monophosphate monohydrate (AMP) with nucleobases and phosphate groups served as bidentate ligands to form water-stable Tb/AMP shell through self-assembled chemistry, in which Fe_3O_4 nanoparticles were in-situ incorporated as guest to form the Fe_3O_4@Tb/AMP core-shell nanoparticles, as shown in Scheme 1a. As nano-adsorbents, the magnetic properties and selective adsorption properties of as-prepared Fe_3O_4@Tb/AMP core-shell nanoparticles were then investigated by batch experiments. The selectivity of Fe_3O_4@Tb/AMP core-shell nanoparticles towards anionic AR/CR rather than cationic dye was studied and the probable mechanism was investigated (Scheme 1a and b). Besides, effects of initial solution pH, salt concentration and adsorbent dosage on adsorption behavior were examined. Moreover, mechanisms with adsorption kinetic, isotherm, thermodynamic were measured and discussed. The regenerability and recyclability of core-shell nanoparticles was assessed via cycling experiment. Finally, under the optimal condition, the practical application of the developed Fe_3O_4@Tb/AMP core-shell nanoparticles for selective removal of anionic dyes from colored wastewater was testified.

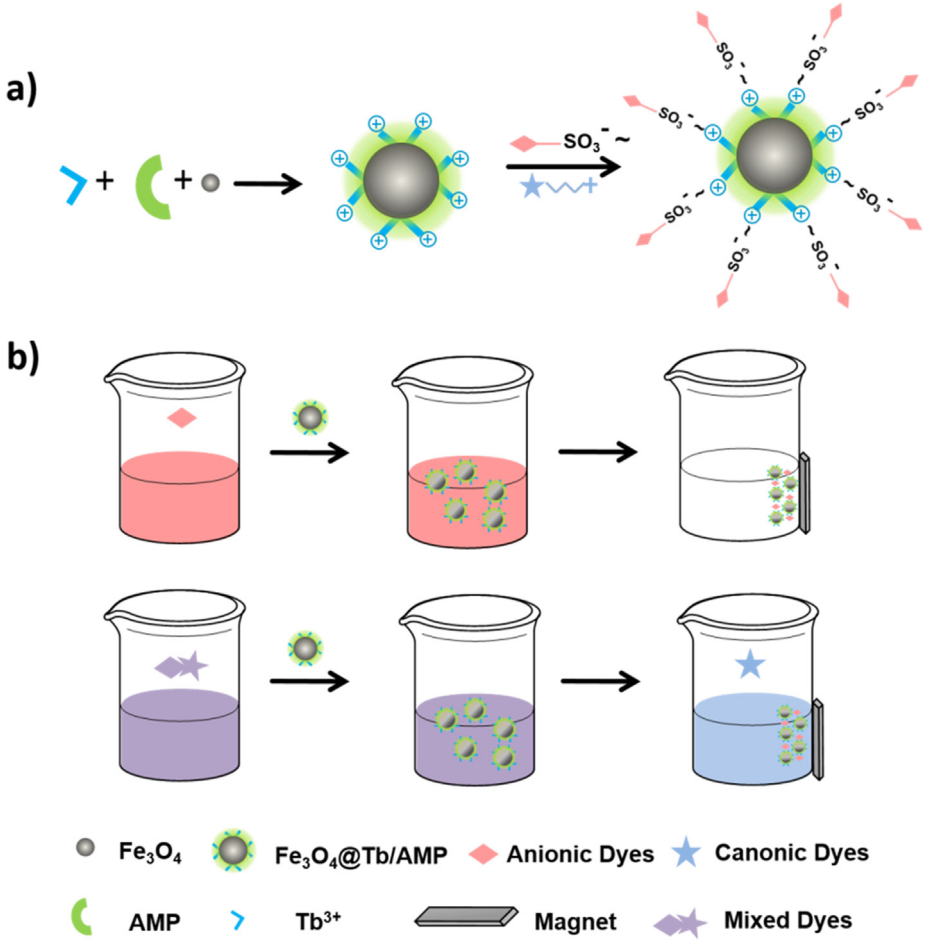

Scheme 1. (a) Schematic illustration for the fabrication of Fe_3O_4@Tb/AMP core-shell nanoparticles. (b) Schematic illustration for selective removal of anionic dyes by using magnetic Fe_3O_4@Tb/AMP ICP core-shell nanoparticles.

2. Experimental

2.1. Materials and reagents

Terbium nitrate pentahydrate ($Tb(NO_3)_3{\cdot}5H_2O$), Alizarin Red (AR), Congo Red (CR) and iron oxide magnetic nanoparticles (Fe_3O_4) were purchased from Aladdin (Shanghai, China). Adenosine 5′-monophosphate monohydrate (AMP) was purchased from Sigma-Aldrich (St. Louis, MO, USA). N-2-Hydroxyethylpiperazine-N'-2-ethane-sulfonic acid (HEPES) was obtained from Sangon Biotech Co. Ltd. (Shanghai, China). Methylene Blue (MB) and Malachite Green (MG) were obtained J & K. (Beijing, China). All chemicals were analytical grade reagents at least and used without further purification. All aqueous solutions were prepared with Milli-Q water (18.2 MΩ cm). Unless otherwise noted, all experiments were carried out at room temperature.

2.2. Synthesis of Fe_3O_4@Tb/AMP core-shell nanoparticles

Initially, the encapsulation of Fe_3O_4 nanoparticles into the Tb/AMP shell was carried out by the following procedures. Briefly, the aqueous solution of $Tb(NO_3)_3{\cdot}5H_2O$ (10 mL, 10 mM) was added into 10 mL HEPES buffer (0.1 M, pH 7.4) containing AMP (10 mM) and magnetic iron oxide nanoparticles (20 mg) under ultrasonication [29]. Within a minute, a dark-brown precipitation was obtained and the collected precipitation was then centrifuged and washed with water for several times. Here, we need to mention that the amount of the "core" Fe_3O_4 nanoparticles was optimized as 1.0 mg mL^{-1}, as demonstrated in Fig. S1.

Supplementary data associated with this article can be found, in the online version, at https://doi.org/10.1016/j.apsusc.2018.08.122.

2.3. Characterization

The size and morphology of as-prepared Fe_3O_4@Tb/AMP core-shell nanoparticles were characterized by Transmission Electron Microscopy (TEM) and Energy Dispersive Spectrometer (EDS) (JEOL 2100F, Japan). Magnetic measurements were performed on PPMS-9T (EC-II) Physical Property Measurement System (Quantum Design, USA) at 298 K. The zeta potential was analyzed using a Malvern Zen 3600 Zetasizer (Malvern Instruments, United Kingdom). UV–vis spectra were recorded on a UV-1800 spectrophotometer (Shimadzu, Japan) and photographs were captured by a Canon IXUS 951S digital camera.

2.4. Adsorption study

To evaluate the adsorption behavior of Fe_3O_4@Tb/AMP core-shell nanoparticles, the dye adsorption study was performed using batch experiments. Firstly, 5000 mg L^{-1} standard reserving solution for the dye was prepared by dissolving 500 mg dye powders with Milli-Q water in 100 mL volumetric flask. Then the dye solutions were simply prepared by diluting the standard reserving solution with Milli-Q water before the adsorption experiment. During the adsorption study, we investigated the UV–vis spectrum of the dyes at different conditions and the dye concentrations could be determined by Beer–Lambert law directly, because the amount of absorbed light of dye solution is directly related to its concentration, as shown in Eq. (1) [32].

$$A = \varepsilon bc \tag{1}$$

Here, A is the absorbance; ε is the molar absorptivity; b is the path length (here is the width of the quartz cell containing the dye solution); c is the concentration of the compound in solution.

The adsorption efficiency was calculated as Eq. (2) [33]:

$$\text{Adsorption efficiency} = \frac{(C_0 - C_t)}{C_0} \times 100\% \tag{2}$$

where C_0 (mg L^{-1}) is the initial concentration of dye; C_t (mg L^{-1}) is the residual concentration of dye. Because the initial concentration of the studied dyes in this work had been chosen in Beer Lambert linear range, instead of Eq. (2) the following equation was used [34]:

$$\text{Adsorption efficiency} = \frac{(A_0 - A_t)}{A_0} \times 100\% \tag{3}$$

where A_0 is the maximum adsorption peak of the dye at their initial concentration; and A_t equals the absorbance of these solutions after the removal process at different conditions.

The effect of initial pH value on the adsorption of dyes was performed by dispersing 3.0 mg Fe_3O_4@Tb/AMP core-shell nanoparticles into 1 mL dye solution with different pH ranging from 2.0 to 9.0. To determine the effect of ionic strength, the adsorption study was carried out by changing the salt concentration of NaCl, $NaNO_3$ and Na_2SO_4 from 0 to 1.0 M.

The adsorbent dosage on dynamic behavior of adsorption was next examined by adding different amount of Fe_3O_4@Tb/AMP core-shell nanoparticles (0–10.5 mg) into 1.0 mL dye solution.

The kinetics of dye adsorption was conducted by mixing 120 mg Fe_3O_4@Tb/AMP core-shell nanoparticles with 40 mL dye solution (800 mg L^{-1} for AR and 1600 mg L^{-1} for CR) in a thermostatic shaker MTH-100. The concentrations of dye were then measured at the end of 1, 2, 3, 4, 5 min.

The adsorption isotherm studies were also conducted by adding 3 mg of Fe_3O_4@AMP/Tb nanoparticles into 1 mL dye solution with the concentration ranging from 100 mg L^{-1} to 1000 mg L^{-1} for AR, and 400 mg L^{-1} to 2600 mg L^{-1} for CR. The mixture was stirred in a thermostatic shaker MTH-100, and then the dyes were separated immediately from the aqueous phase by an external magnet. The adsorption efficiency was calculated as Eq. (4) [33]:

$$\text{Adsorption efficiency} = \frac{C_0 - C_e}{C_0} \times 100\% \tag{4}$$

And the equilibrium uptake was calculated using Eq. (5) [35]:

$$q_e = (C_0 - C_e) \times \frac{V}{m} \tag{5}$$

where q_e (mg g^{-1}) is the equilibrium adsorption capacity; C_0 (mg L^{-1}) is the initial concentration of dye; C_e (mg L^{-1}) is the residual dye concentration in solution at equilibrium; V (L) is the volume of the dye solution and m (g) is the weight of adsorbent.

The thermodynamic parameters of the adsorption process were further obtained by running the adsorption system at 298 K, 313 K, and 328 K, with other conditions unchanged. The residual dye concentration was measured via UV–vis spectrophotometer after a pre-determined adsorption time.

2.5. Desorption and reusability

The regeneration of the magnetic Fe_3O_4@Tb/AMP core-shell nanoparticles for AR/CR was evaluated through five successive cycles based on two experimental procedures. Firstly, 12 mg Fe_3O_4@Tb/AMP core-shell nanoparticles was mixed with 4 mL dye solution (100 mg L^{-1} for AR and 200 mg L^{-1} for CR). After magnetic separation, the dye-loaded adsorbents were then added to 8 mL Na_2SO_4 (1 M) aqueous solution for AR and 4 mL methanol/NaCl (2 M) solution with a volume ratio (v/v = 3:1) for CR at the temperature of 310 K. After shaking for 2 h, the regenerative adsorbent was washed thoroughly using Milli-Q water and then reused for the subsequent cycles.

2.6. Selective separation of anionic dyes from colored wastewater

The selective removal of anionic dyes from colored wastewater was investigated under optimal adsorption conditions. Firstly, a mixed aqueous solution of the anionic and cationic dye (100 mg L^{-1} AR/20 mg L^{-1} MB in pH 5 or 200 mg L^{-1} CR/100 mg L^{-1} MG in pH 6) was

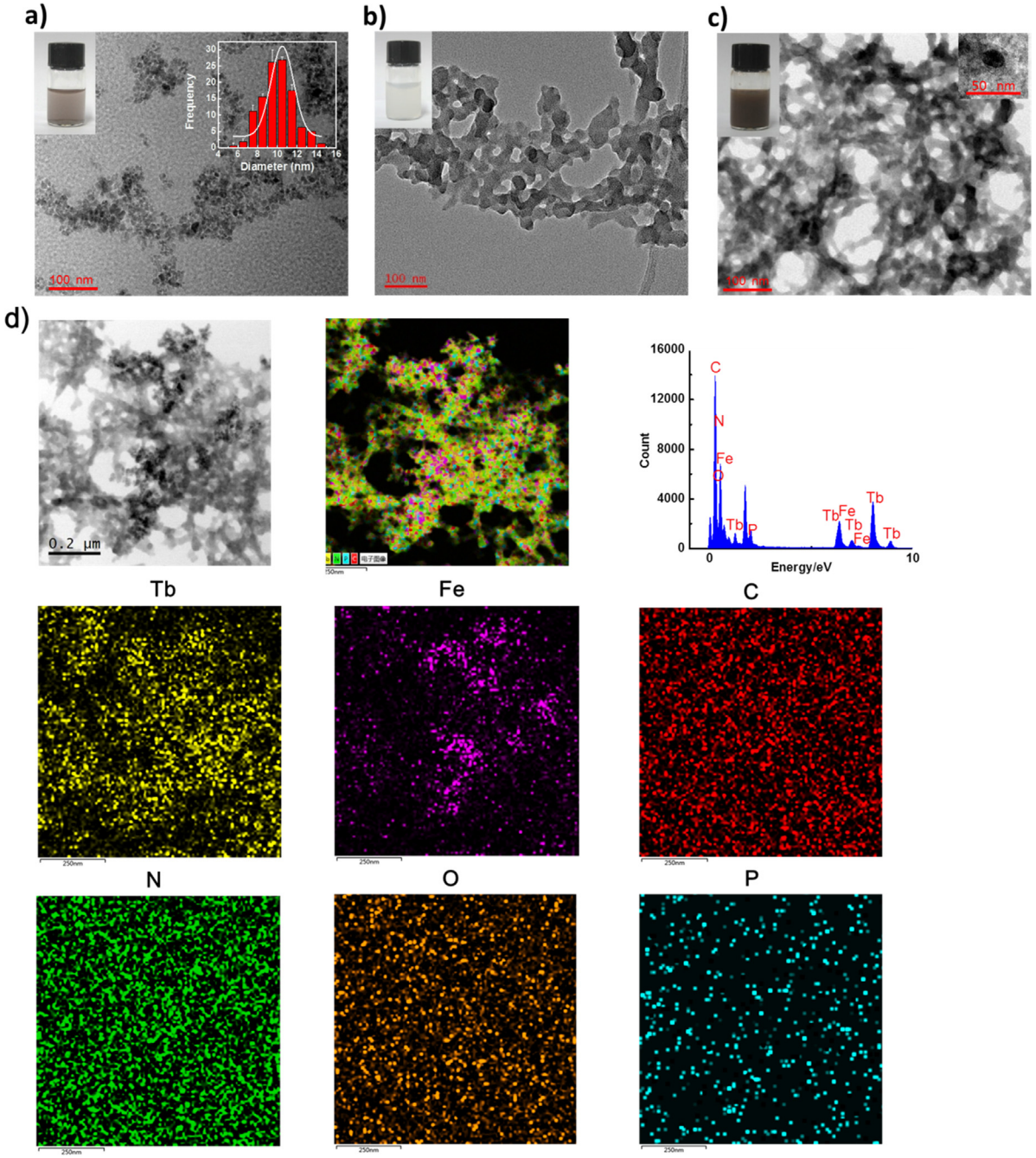

Fig. 1. (a) TEM images of Fe_3O_4 nanoparticles. Inset: photographs (left) and the size distributions (right) of Fe_3O_4 nanoparticles; (b) TEM images of Tb/AMP ICP nanoparticles. Inset: photographs; (c) TEM images of Fe_3O_4@Tb/AMP core-shell nanoparticles. Inset: photographs (left) and high-resolution TEM images (right); (d) TEM-EDS micrograph and the elemental analysis of Fe_3O_4@Tb/AMP core-shell nanoparticles.

formed. Then 3 mg Fe_3O_4@Tb/AMP core-shell nano-adsorbents was added into 1 mL as-formed dye solution. After magnetic separation, the residual concentration of anionic and cationic dyes was detected by a UV–vis spectrophotometer.

Selective removal of anionic dyes of wastewater from textile industry was carried out by dispersing 3 mg Fe_3O_4@Tb/AMP core-shell nano-adsorbents directly into 1.0 mL colored wastewater 1 which contained anionic dye, colored wastewater 2 with the addition of AR (100 mg L^{-1}) or CR (200 mg L^{-1}), respectively. After magnetic separation, the anionic dye remained in colored wastewater from textile industry was detected by a UV–vis spectrophotometer.

3. Results and discussions

3.1. Preparation and characterization of Fe_3O_4@Tb/AMP core-shell nanoparticles

Initially, magnetic Fe_3O_4 nanoparticles with uniform size 10.29 ± 3.18 nm were chosen as core (Fig. 1a) and lanthanide based infinite coordination polymers Tb/AMP were selected as shell (Fig. 1b). By taking the advantage of self-adaptive inclusion property of the supramolecular network of Tb/GMP, Fe_3O_4@Tb/AMP core-shell nanoparticles were synthesized through “one-pot” reaction easily. The as-formed Fe_3O_4@Tb/AMP core-shell nanoparticles exhibited a dark-brown color and well-dispersed in aqueous solution (Fig. 1c, inset, left).

To further verify the encapsulation of Fe_3O_4 nanoparticles into Tb/AMP shell, we investigated transmission electron microscopy (TEM) and transmission electron microscope-energy dispersive spectroscopy (TEM-EDS) of Fe_3O_4@Tb/AMP core-shell nanoparticles. Fig. 1c clearly showed that Fe_3O_4 nanoparticles were surrounded by the amorphous shell of Tb/AMP ICPs with a thickness about 30–40 nm and the size of whole core-shell nanoparticles was about 50–60 nm (Fig. 1c, inset, right). Moreover, TEM-EDS micrograph and the elemental analysis of the Fe_3O_4@Tb/AMP core-shell nanoparticles showed the presence of Tb, Fe, C, N, O and P elements, which was also indicative of the successful formation of Fe_3O_4@Tb/AMP core-shell nanoparticles (Fig. 1d).

The magnetic property of as-formed Fe_3O_4@Tb/AMP core-shell nanoparticles was next characterized by a vibrating sample magnetometer and compared with the core Fe_3O_4 nanoparticles. As shown in Fig. 3, the magnetic hysteresis loops indicate the magnetic saturation (Ms) values for Fe_3O_4 nanoparticles and Fe_3O_4@Tb/AMP core-shell nanoparticles are 52.61 emu g^{-1}, 19.24 emu g^{-1}, respectively. The decrease of Ms for Fe_3O_4@Tb/AMP core-shell nanoparticles may attribute to the local environmental changes of Fe_3O_4 nanoparticles caused by the wrapping of Tb/GMP networks [36]. Nevertheless, the Ms value of core-shell nanoparticles was sufficient for the immediate removal the core-shell nanoparticle by using an external magnet easily (Fig. 2, inset) [37,38].

The adsorption property of as-formed Fe_3O_4@Tb/AMP core-shell nanoparticles was further examined. Alizarin Red (AR, anthraquinone) and Congo Red (CR, azo) which represent two major of reactive dyes were used as models for anionic dyes. Methylene Blue (MB) and Malachite Green (MG) with different UV–vis absorption from AR and CR were chosen as models for cationic dyes. As shown in Fig. 3, the sole addition of the Fe_3O_4 nanoparticles into either anionic or cationic dye solution does not cause obvious change either in the color or in the UV–vis spectra after magnetic separation, indicating that the Fe_3O_4 nanoparticles cannot adsorb any dyes. With the addition of Fe_3O_4@Tb/AMP core-shell nanoparticles, both the color and the characteristic peak of AR/CR disappeared after separation by permanent magnet, while that for MB/MG remained almost the same, suggesting the selective absorption property of Fe_3O_4@Tb/AMP core-shell nanoparticles towards anionic AR/CR rather than cationic MB/MG, and this selectivity may result from the shell. The as-formed Fe_3O_4@Tb/AMP core-shell nanoparticles well-combined the inherent properties of both the core Fe_3O_4 nanoparticles and the shell Tb/AMP, are very promising to realize the selective adsorption and magnetic separation of anionic dyes from colored wastewater in a cost-effective way.

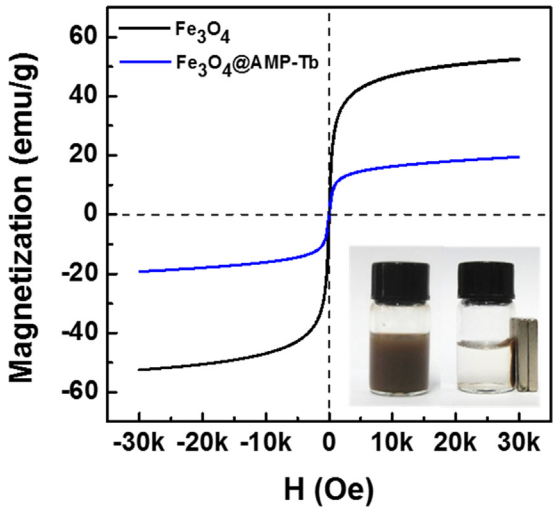

Fig. 2. Magnetic hysteresis curves of Fe_3O_4 and Fe_3O_4@AMP/Tb core-shell nanoparticles at 298 K. Inset: photographs of the separation of Fe_3O_4@AMP/Tb core-shell nanoparticles from solution by a permanent magnet.

To gain more insight into the selective adsorption mechanism, Fourier transfer infrared (FT-IR) spectra of Fe_3O_4@Tb/AMP core-shell nanoparticles, AR/CR before and after adsorption were investigated. As shown in Fig. 4, for Fe_3O_4@Tb/AMP core-shell nanoparticles (black curve), the peak at 1477 cm^{-1} is attributed to the N7-C8 stretching vibration in the adenine moieties, 1109 and 994 cm^{-1} are ascribed to $\nu_{as}PO_4$ and ν_sPO_4 stretching vibration of phosphate groups, respectively [21]. In addition, the absorption at 580 cm^{-1} is assigned to the stretching of Fe-O vibration, again validating the encapsulation of the Fe_3O_4 nanoparticles in Tb/AMP shell [39]. When AR/CR was absorbed on Fe_3O_4@Tb/AMP core-shell nanoparticles, the corresponding peak wavenumbers slightly shifted to 1478, 1110, 993, and 1478, 1111, 996 cm^{-1}, respectively (blue curve), demonstrating that the adsorption of AR/CR had little effect on the structural integrity of Fe_3O_4@Tb/AMP core-shell nanoparticles. The minor changes in the wavenumber could be attributed to weak binding interactions between AR/CR and Tb/AMP. For free AR (Fig. 4a), the characteristic peaks at 1665, 1637 cm^{-1} are attributed to C═O stretching vibration, the peaks at 1589, 1439 cm^{-1} are due to the C═C bonds in benzene ring and the bands at 1159, 1068, 639 cm^{-1} are due to the sulfonic groups [40]. For CR (Fig. 4b), the characteristic peak appeared at 1583 cm^{-1} is contributed to N═N stretching, the peaks at 832, 750, 699 cm^{-1}, are attributed to aromatic skeletal groups; the peaks at 1350 cm^{-1}, is due to S-O stretching; the peaks at 1226, 1178, 1064, 640 cm^{-1}, are corresponding to S═O stretching in sulfonate groups [41,42]. Interestingly, after adsorption, the characteristic peaks of AR/CR could not be observed, suggesting that the anionic dyes may locate interior of Tb/AMP shell rather than simply adsorbed on the surface, thus the vibration of AR/CR was restrained due to the shielding effect of ICPs shell [43]. From all of these results demonstrated above, we concluded the porosities, highly structural flexibility of Tb/AMP shell would be favorable for defusing and accommodating anionic dyes into the network and large coordination number of the positive trivalent lanthanide ions facilitated the possible binding of anionic dyes to achieve the selectivity.

3.2. Optimization for adsorption of anionic AR/CR.

3.2.1. Effect of initial pH

To realize the selective removal of anionic dyes from wastewater, the adsorption experimental conditions were optimized. pH values, which could change the degree of the ionization of the dyes and the surface charge of Fe_3O_4@Tb/AMP core-shell nanoparticles, was firstly taken into account [44]. As shown in Fig. 5a, the adsorption efficiency reaches the maximum at pH 5.0 for AR (94.02%) and at pH 6.0 for CR (96.35%). To clarify the impact of pH on AR/CR adsorption more clearly, the isoelectric point (IEP) of the Fe_3O_4@Tb/AMP core-shell nanoparticles was determined to be 6.1 (Fig. 5b). Therefore, the surface charge of Fe_3O_4@Tb/AMP core-shell nanoparticles would be positive, when pH was lower than 6.1. With the presence of sulfonate groups, both AR and CR are anionic in nature, as a result, in acidic environment, electrostatic interaction between the positively charged Fe_3O_4@Tb/AMP core-shell nanoparticles and negatively charged dye molecules advanced AR/CR adsorption. However, the excessive hydrogen ions might compete with the magnetic ICP core-shell nanoparticles, leading to the adsorption capacity declined with decreasing of pH under IEP. Conversely, when pH was higher than IEP, the excess of negative-charged hydroxyl ions (OH^-) interacted with the adsorbent, consequently, the repulsive interactions between Fe_3O_4@Tb/AMP core-shell nanoparticles and AR/CR enhanced, thus the adsorption efficiency of dye molecules decreased with increasing pH higher than IEP.

3.2.2. Effect of salt concentration

Actually, the wastewater from textile and dyestuff industries was a mixture of dyes and large amounts of negative ions, such as NO_3^-, SO_4^{2-} and Cl^-. The anion exchange mechanism between the salt anion and anionic dye molecules with the cationic nano-absorbents via ionic

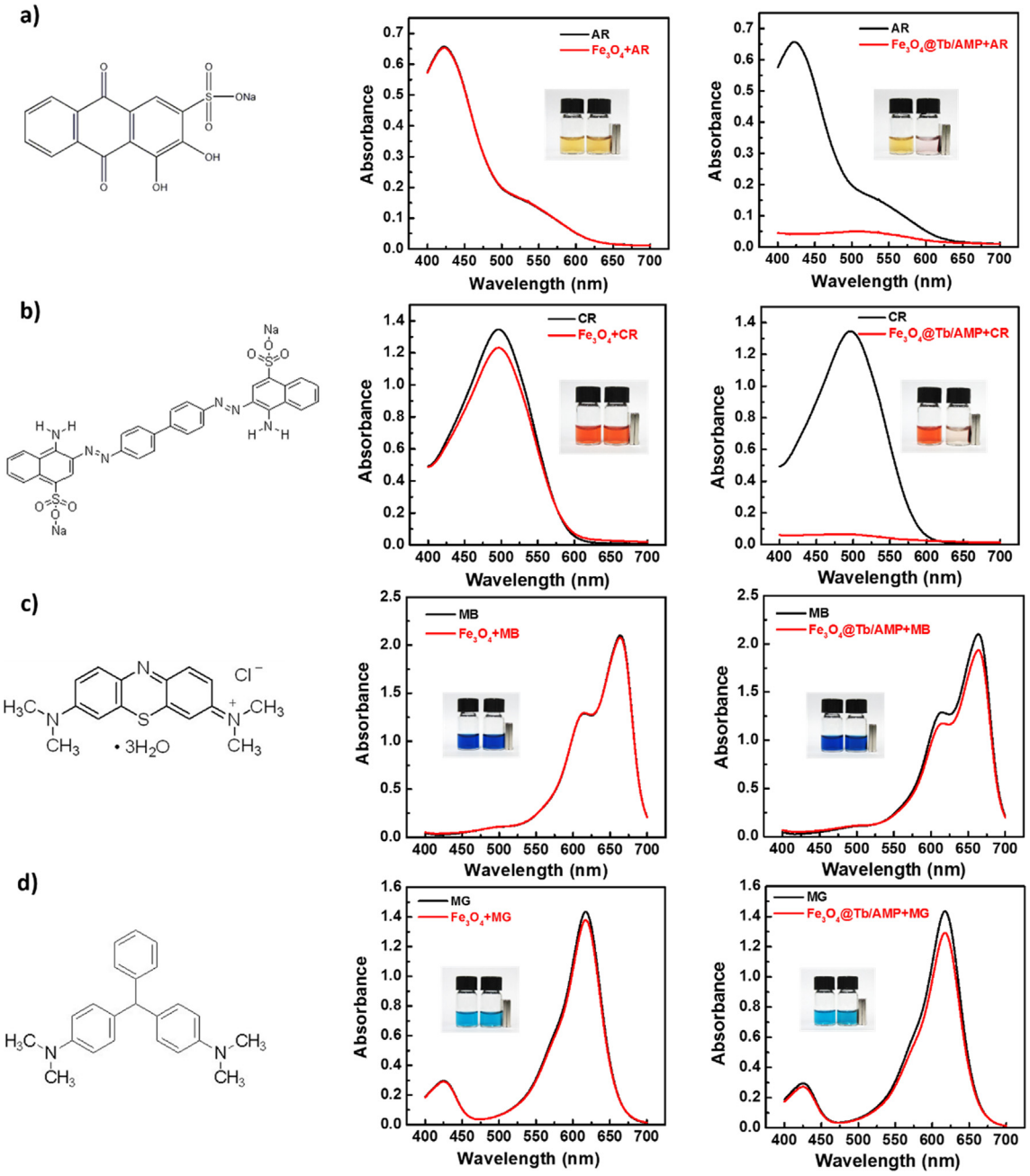

Fig. 3. Structures (left), UV–vis spectra and photographs (inset) of the dye solution without and with presence of Fe_3O_4 nanoparticles (middle) and Fe_3O_4@Tb/AMP core-shell nanoparticles (right). AR (100 mg L^{-1}) (a); CR (200 mg L^{-1}) (b); MB (20 mg L^{-1}) (c); MG (100 mg L^{-1}) (d).

interactions may retard the adsorption performance [45]. Based on this, NaCl, $NaNO_3$ and Na_2SO_4 with different concentration ranging from 0 M to 1.0 M were added into dye solution and the effect of salt concentration was tested, respectively. As shown in Fig. 5c, d, the increase in the concentration of NaCl or $NaNO_3$ from 0 M to 1.0 M shows little impact on adsorption efficiency of Fe_3O_4@Tb/AMP core-shell nanoparticles toward anionic dyes, especially for CR. However, with increasing the concentration of Na_2SO_4, AR/CR adsorption efficiency decreased obviously. This difference may be derived from both the competitive binding interaction between SO_4^{2-} and the sulfonic group of AR/CR towards Tb^{3+} and the stronger repulsive effect of SO_4^{2-} towards AR/CR than that of Cl^-, NO_3^-. Furthermore, the concentration of SO_4^{2-} showed less effect on the CR uptake by Fe_3O_4@Tb/AMP core-shell nanoparticles than that on AR, which may due to the two sulfonic groups of CR increased the repulsive effect of the nanoabsorbents to SO_4^{2-}.

3.2.3. *Effect of adsorbent dosage*

It is well-known that the adsorbent dosage plays very important roles in removing AR/CR dyes from aqueous solution. Fig. 6 represented the effect of Fe_3O_4@Tb/AMP core-shell nanoparticles dosage on AR/CR adsorption. For both dyes, the adsorption efficiency became more and more efficient upon increasing the adsorption amount from 0 to 3 mg and then was hardly influenced by further increasing the adsorbent dosage. The maximum removal of AR (100 mg L^{-1}, 94.16%) and CR (200 mg L^{-1}, 95.96%) were achieved in the presence of 3 mg Fe_3O_4@Tb/AMP core-shell nanoparticles.

This phenomenon can be elucidated as following: at the first stage, with increasing the dosage of Fe_3O_4@Tb/AMP core-shell nanoparticles, higher adsorbent surface and larger availability adsorption sites of

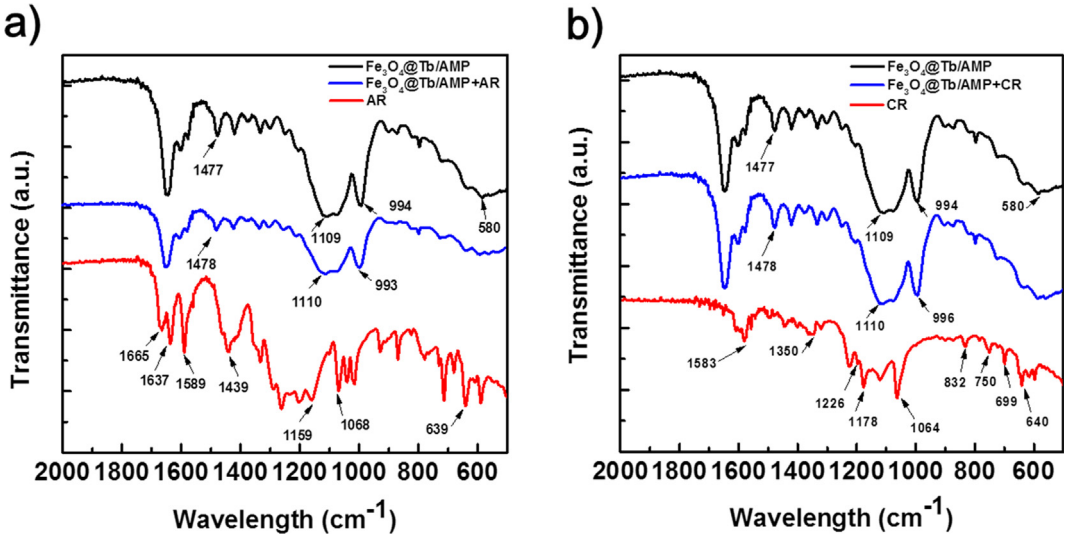

Fig. 4. FTIR spectra of Fe_3O_4@Tb/AMP core-shell nanoparticles, free dyes and dye adsorbed Fe_3O_4@Tb/AMP core-shell nanoparticles. AR (a) and CR (b).

Fe_3O_4@Tb/AMP core-shell nanoparticles advanced dye adsorption. Nevertheless, with subsequent increasing the dosage of adsorbent, overlapping or aggregation of adsorption sites decreased the available binding sites of per unit adsorbent. Consequently, the total adsorption sites approached to saturate and the rate of adsorption tended to reach equilibrium [46].

3.3. Adsorption kinetics, isotherm and thermodynamic studies

To realize selective adsorption and separation of anionic dyes from

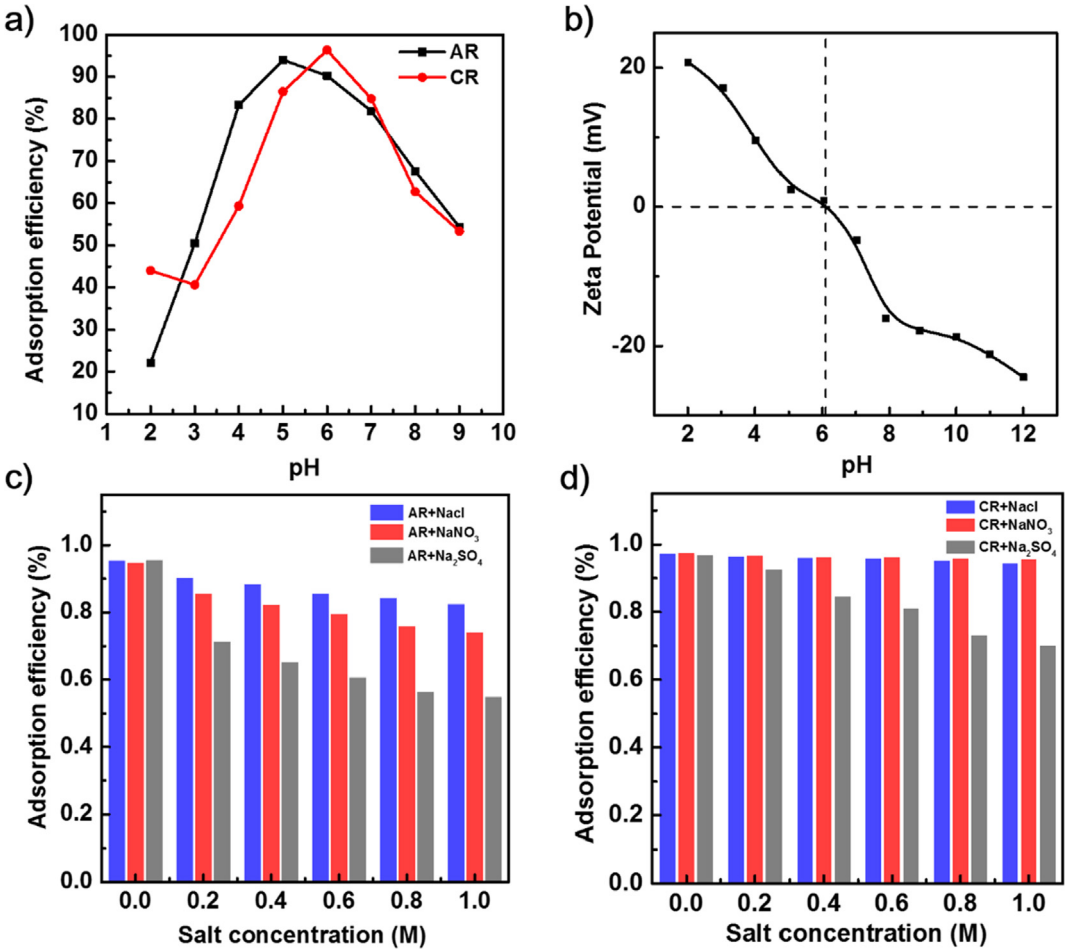

Fig. 5. (a) Effect of pH on adsorption efficiency. (b) IEP of the Fe_3O_4@Tb/AMP core-shell nanoparticles; (c) Effect of NaCl, $NaNO_3$ and Na_2SO_4 concentration on adsorption efficiency towards AR (c) and CR (d) (Conditions: adsorbent dosage, 3 mg; initial dye concentration, AR: 100 mg L^{-1} and CR: 200 mg L^{-1}; and at the temperature of 298 K).

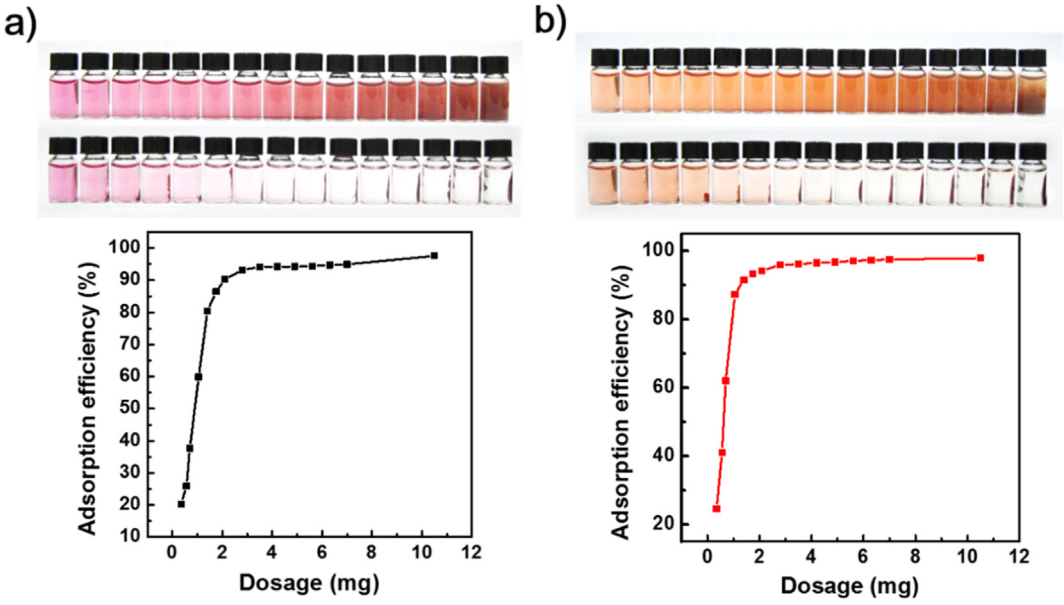

Fig. 6. Effect of the dosage of Fe_3O_4@Tb/AMP core-shell nanoparticles on adsorption efficiency of AR (a) and CR (b) (Upper: photographs).

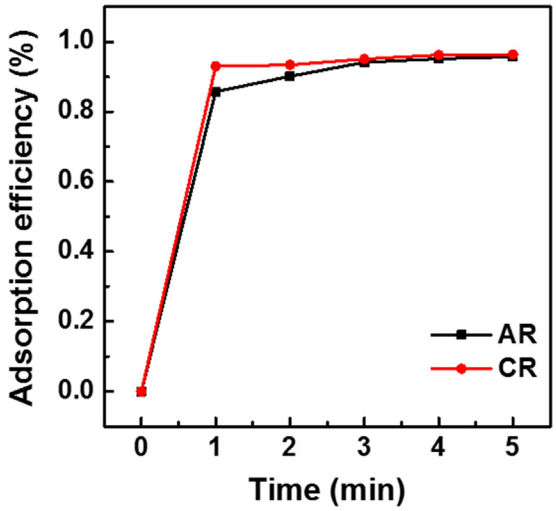

Fig. 7. Kinetics of AR/CR removal by Fe_3O_4@Tb/AMP. (Conditions: initial solution pH, AR: pH = 5 and CR: pH = 6; Buffer concentration: 0.05 M; and at the temperature of 298 K).

colored wastewater, adsorption kinetics which correlated with treatment cost in terms of adsorbent dose per unit time were studied firstly from the practical viewpoint. As shown in Fig. 7, both AR and CR achieve adsorption equilibriums within five minutes and the adsorption efficiency is around 96%. To verify the mechanism of fast adsorption and its potential rate-controlling step, intra-particle diffusion model, pseudo-first-order and pseudo-second-order models were employed for Fe_3O_4@Tb/AMP core-shell nanoparticles (Fig. S2). As is shown in Fig S2a and b, when the Weber and Morris intra-particle diffusion model is employed, the plotted line does not pass through the origin and the correlation was poor (Table S1), indicating that intra-particle diffusion is not the rate limiting step [47]. This is also corroborated by the fact that the Tb/GMP supramolecular networks could accommodate anionic dyes by flexibly adapting the shape of guest molecules thus reducing the resistance in the intra-particle diffusion path. The pseudo-first- and second- order models were next performed as a comparison [48,49]. The adsorption kinetics fitted well with the pseudo-second-order and the obtained coefficients (R^2) were almost 1 for both dyes (Fig. S2c, Table S1). This result suggested that chemisorption and/or ion exchange mechanism makes a significant contribution to the overall process kinetics, which showed great coincidence with the results demonstrated above. In addition, the fast kinetics features of Fe_3O_4@Tb/AMP core-shell nanoparticles make it more applicable for practical applications with operational convenience and low cost.

The adsorption isotherm represented the relationship between the removal ability of the adsorbents and the concentration of the dye solution was next investigated. As depicted in Fig. 8a, within the low concentration range, the values of q_e for both dyes increased linearly with increasing the concentration of dye solution at room temperature. However, the linear growth of the adsorption capacities is restricted at higher concentrations, thus the maximum q_e value for AR and CR was up to 345.54 mg g^{-1} and 868.56 mg g^{-1}, respectively. To clarify the adsorption process more clearly, Langmuir and Freundlich isothermal models were employed to evaluate the equilibrium adsorption.

Langmuir isotherm model proposes the monolayer adsorption occurs at specific homogenous sites within the adsorbent. Once a dye molecule occupies a site, no further adsorption will take place at the site [50,51]. The Langmuir equation was shown as Eq. (6) [52]:

$$\frac{C_e}{q_e} = \frac{1}{K_L q_m} + \frac{C_e}{q_m} \tag{6}$$

where q_m (mg g^{-1}) and K_L (L mg^{-1}) are the maximum capacity of the adsorbents and the Langmuir adsorption isotherm model constant associated with adsorbent energy, respectively. By plotting C_e/q_e againstC_e, the value ofq_m could be obtained directly from the slope and then the valve of K_L from the intercept.

For Freundlich isotherm model, it describes the multilayer adsorption occurs on heterogeneous surfaces with a uniform energy distribution, within which additional interaction between adsorbed molecules resulted in an increase of the amount of dye adsorbed on the adsorbents with increasing dye concentration in solution. The Freundlich equation was given as Eq. (7) [52]:

$$\ln q_e = \frac{1}{n}\ln C_e + \ln K_F \tag{7}$$

where K_F (L mg^{-1}) is the Freundlich constant which is connected to the magnitude of adsorption driving force and 1/n is heterogeneity factor. By plotting $\ln q_e$ versus $\ln C_e$, the valve of 1/n and K_F could be calculated from the slope and intercept, respectively. As shown in Fig. 8b, c, the corresponding correlation coefficients (R^2) values of Langmuir model ($R^2 > 0.9910$) are much higher than that of Freundlich model

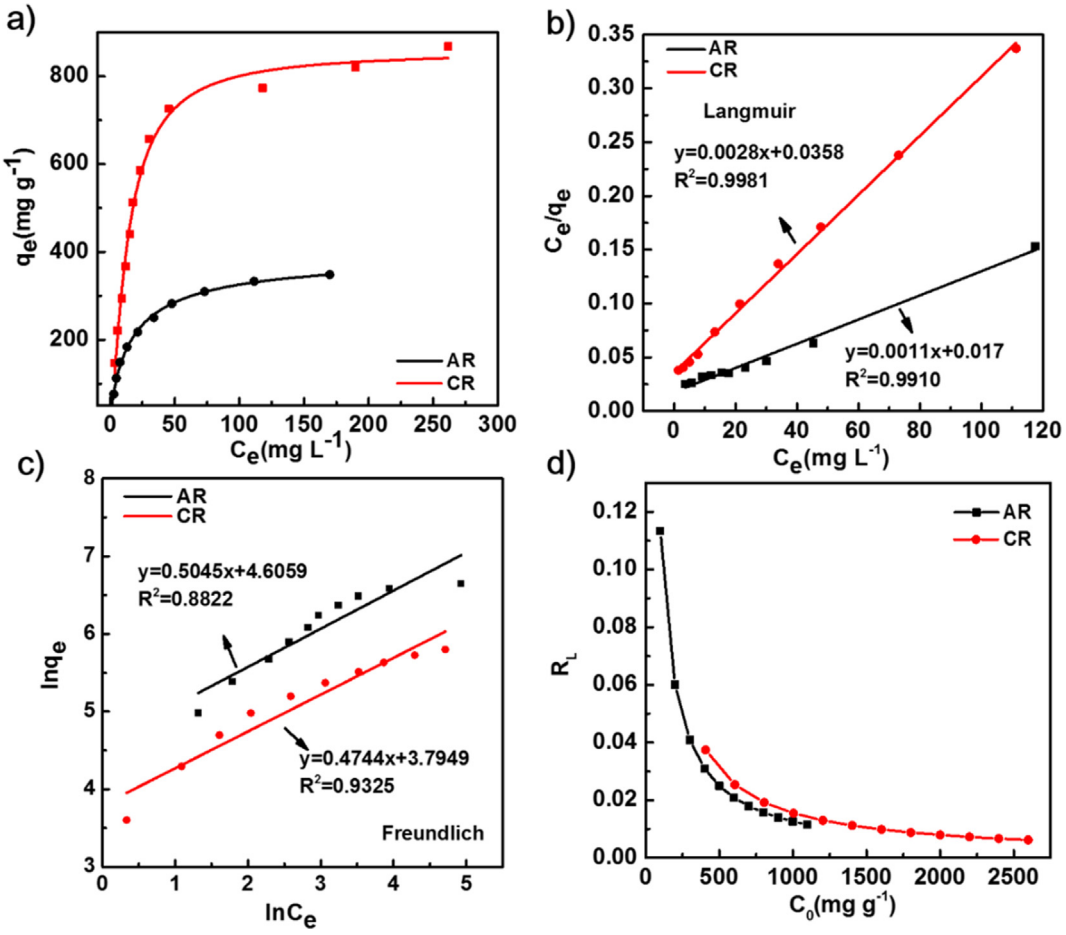

Fig. 8. (a) Adsorption isotherms of AR and CR onto Fe_3O_4@Tb/AMP core-shell nanoparticles; Langmuir Plot (b) and Freundlich Plot (c) for adsorption of AR/CR onto Fe_3O_4@AMP/Tb core-shell nanoparticle; (d) Separation factor for the adsorption of AR/CR Fe_3O_4@Tb/AMP core-shell nanoparticles (Conditions: adsorbent dosage, 3 mg; initial solution pH, AR: pH = 5 and CR: pH = 6; Buffer concentration: 0.05 M; and at the temperature of 298 K).

Table 1
Parameters of adsorption isotherm for Fe_3O_4@Tb/AMP core-shell nanoparticles.

Fitting model	Parameter	Dyes	
		AR	CR
Langmuir	q_{exp}(mg g^{-1})	345.54	868.56
	q_m(mg g^{-1})	357.14	909.09
	K_L(L mg^{-1})	0.0782	0.0647
	R^2	0.9981	0.9910
Freundlich	K_F(mg/g(L/mg$^{1/n}$)	44.47	100.07
	1/n	0.4744	0.5045
	R^2	0.9325	0.8822

(R^2 < 0.9325), indicating that Langmuir isotherm model is more applicable to evaluate the selective adsorption of AR/CR at the specific adsorption sites of Fe_3O_4@Tb/AMP core-shell nanoparticles. Meanwhile, the dye adsorption process is not affected by its own intermolecular interaction between the adsorbed dye molecules. Finally, the adsorption site would reach saturation at high adsorbate concentration, resulting in the equilibrium of the dye adsorbed. According to the simulated Langmuir isotherm data, the maximum adsorption capacity estimated from the linear regression equation is 357.14 mg g^{-1} for AR and 909.09 mg g^{-1} for CR, matching well with the experimental data 345.54 mg g^{-1} and 868.56 mg g^{-1} (Table 1). This result also validated the applicability of Langmuir model to predict the adsorption process. Since the essential features of the Langmuir isotherm can be expressed in terms of a dimensionless constant called separation factor (R_L, also called equilibrium parameter), the value of R_L was further calculated by the following equation Eq. (8) [53]:

$$R_L = \frac{1}{1 + K_L C_0} \tag{8}$$

where the value of C_0 is the initial concentration of dye solution, R_L indicates reaction type: unfavorable ($R_L > 1$), linear ($R_L = 1$), favorable ($0 < R_L < 1$), and irreversible ($R_L = 0$).

The calculated R_L which reflected the tightness of connection between the adsorbent and the adsorbate are smaller than 1 for both AR and CR (Fig. 8d), indicating the adsorption process was favorable [54]. Moreover, the value of R_L for CR is smaller than that for AR, suggesting the adsorption process of Fe_3O_4@Tb/AMP core-shell nanoparticle towards CR is the more favorable than AR under the experimental condition, which was consistent with the actual experimental results demonstrated above.

Table 2 presented the comparison of Fe_3O_4@Tb/AMP core-shell nanoparticle we developed and other adsorbents reported before. It could be found out that the q_m of Fe_3O_4@Tb/AMP nanoparticles calculated from Langmuir isotherm model for removal of AR/CR exhibited great superiority over other adsorbents, which substantially validated the further application of Fe_3O_4@Tb/AMP nano-adsorbents for selective treatment of anionic dyes in colored wastewater from textile industry.

The thermodynamic parameters, which not only reflected the relationship between AR/CR adsorption and temperature, but also gave in-depth information about the inherent energetic changes during

Table 2
Comparison of q_m of various adsorbents for AR/CR.

Dye	Adsorbents	q_m(mg/g)	References
Alizarin red	CS-IMBTESPEDA-SBA-15	50.25	[55]
Alizarin red	MAC nano-composite	108.69	[56]
Alizarin red	Fe_3O_4@PPy NPs	116.30	[57]
Alizarin red	Au-NPs-AC	123.15	[58]
Alizarin red	**Fe_3O_4@AMP-Tb**	**357.14 mg/g**	**Present study**
Congo red	NiAl-S_1 LDH	120.50	[59]
Congo red	DP Mn_2O_3-carbon-PVP	125.60	[60]
Congo red	Hierarchical porous ZnO	334.00	[61]
Congo red	MoS_2- rGO	415.90	[62]
Congo red	**Fe_3O_4@AMP/Tb**	**909.09 mg/g**	**Present study**

adsorption process were next determined from the adsorption isotherms at different temperatures. Standard Gibbs free energy change (ΔG^θ, kJ mol^{-1}) is calculated with Eq. (9). Standard enthalpy change(ΔH^θ, kJ mol^{-1}) and standard entropy change (ΔS^θ, J mol^{-1} K^{-1}) are calculated from the slope and the intercept of the plot of ln K^θ versus 1/T using the van' Hoff Eq. (10) [63].

$$\Delta G^\theta = -RTlnK^\theta \tag{9}$$

$$lnK^\theta = \frac{\Delta S^\theta}{R} - \frac{\Delta H^\theta}{RT} \tag{10}$$

where T (K) is the temperature in Kelvin, R (8.314 J mol^{-1} K^{-1}) is universal gas constant and K is the thermodynamic equilibrium constant for the adsorption process, which can be calculated from the ratio of the equilibrium adsorption capacity (q_e) to the equilibrium concentration of the solution (C_e).

The plot of lnK^θ vs 1/T for the adsorption of AR/CR onto Fe_3O_4@Tb/AMP core-shell nanoparticles at 298, 313, 328 K are shown in Fig. S3 and the calculated thermodynamic parameters are shown in Table 3. Generally, the negative ΔG at various temperatures indicated that the adsorption of AR/CR onto magnetic Fe_3O_4@Tb/AMP core-shell nanoparticles was spontaneous. The positive ΔS suggested the adsorption process led to the increase of randomness and the positive ΔH implied this adsorption process was endothermic, which meant that when the temperature was higher, the maximum adsorption capacities could further be improved as shown in Eq. (11) [64].

$$ln\frac{K_2^\theta}{K_1^\theta} = \frac{\Delta H^\theta}{R}\left(\frac{1}{T_1} - \frac{1}{T_2}\right) \tag{11}$$

3.4. Desorption and reusability

As a novel water purification technology for colored wastewater treatment with commercial feasibility, it requires the developed adsorbents bear advantage of the adsorption ability not only in rapid adsorption rate, high removal capacity, but also more especially in the recyclability. In this study, a simple method was applied to regenerate dye-adsorbed Fe_3O_4@Tb/AMP ICP core-shell nanoparticles. Typically,

Table 3
Thermodynamic parameters for the adsorption of AR/CR onto Fe_3O_4@Tb/AMP core-shell nanoparticles at different temperatures.

Dye	Co (mg/L)	Thermodynamic parameters			
		T (K)	ΔG (kJ mol^{-1})	ΔH (kJ mol^{-1})	ΔS (J mol^{-1} K^{-1})
AR	800	298	−3.4158	6.5032	33.2884
	800	313	−3.9161		
	800	328	−4.4154		
CR	1600	298	−5.7280	13.1486	63.3444
	1600	313	−6.7094		
	1600	328	−7.6284		

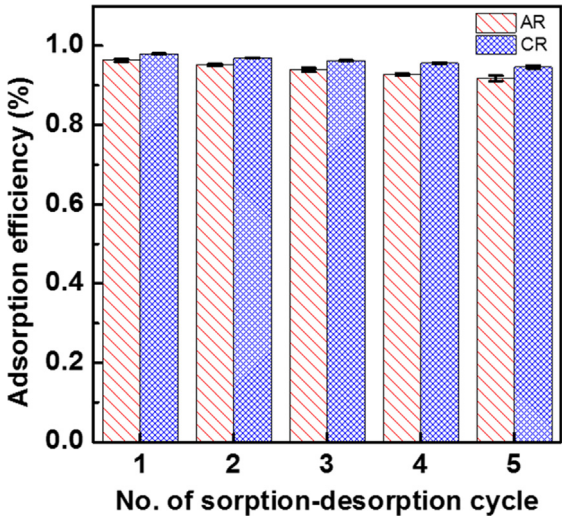

Fig. 9. Cyclic regeneration of Fe_3O_4@Tb/AMP core-shell nanoparticles. The desorption solvent: 8 mL Na_2SO_4 aqueous solution (1 M) for AR and 4 mL methanol/NaCl (2 M) solution with a volume ratio (v/v = 3:1) for CR.

8 mL Na_2SO_4 aqueous solution (1 M) for AR and 4 mL methanol/NaCl (2 M) solution with a volume ratio (v/v = 3:1) for CR were used as desorption solvent, respectively. As depicted in Fig. 9, the adsorption efficiency of AR and CR were as high as 91.76% and 95% after 5 consecutive cycles, suggesting that Fe_3O_4@Tb/AMP core-shell nanoparticles with good regeneration and reusability are economically sustainable in colored wastewater management. Note that, to obtain the maximum desorption efficiency, desorption solvents have already been optimized during the regeneration process, as demonstrated in Fig. S4.

3.5. Selective adsorption of anionic dyes from colored wastewater

Having demonstrated the great adsorption ability and reusability of Fe_3O_4@Tb/AMP nanoparticles, the selective adsorption of anionic dye from the mixed dye solution was investigated under the optimal condition. 3 mg Fe_3O_4@Tb/AMP nanoparticles were added into the mixtures of AR/MB (1.0 mL, 100 mg L^{-1}/20 mg L^{-1} in pH 5) and CR/MG (200 mg L^{-1}/100 mg L^{-1} in pH 6), respectively. As shown in Fig. 10a, after adsorption and magnetic separation, the dark green color of AR/MB changes into greenish blue and UV–vis spectra of the mixture suggested that the characteristic peak of AR at 423 nm disappeared while that for the MB at 672 nm was not impressive. For CR/MG mixture, after adsorption, the light green color turns into light blue and the similar change of characteristics peak could also been observed (Fig. 10b). These features indicated that the selective removal of anionic dyes from mixed dye solution could be realized by Fe_3O_4@Tb/AMP nanoparticles easily.

To further demonstrate the practical application of Fe_3O_4@Tb/AMP nanoparticles for selective removal of anionic dyes, two colored wastewater from textile industry were then testified. As shown in Fig. 10c, with the presence of Fe_3O_4@Tb/AMP nano-adsorbents, not only the color but also the characteristic absorption peak at 578 nm of colored wastewater 1 (which contained anionic dye) diminished, indicating the removal of the dye clearly (99.31 ± 0.46%). As far as the universality of the nano-adsorbents was considered, AR (100 mg L^{-1}) or CR (200 mg L^{-1}) were added standardly to colored wastewater 2, which is complex and may be without the presence of anionic dyes. As shown in Fig. 10d, e, the color and the UV–vis absorption of AR/CR in colored wastewater 2 also diminished and the adsorption efficiency were as high as 98.81 ± 2.15% for AR and 99.53 ± 3.06% for CR, as presented in Table 4. All of these properties ensured the reliability of the magnetic Fe_3O_4@Tb/AMP ICP core-shell nanoparticles for selective removal of anionic dyes from colored wastewater directly, which pave a

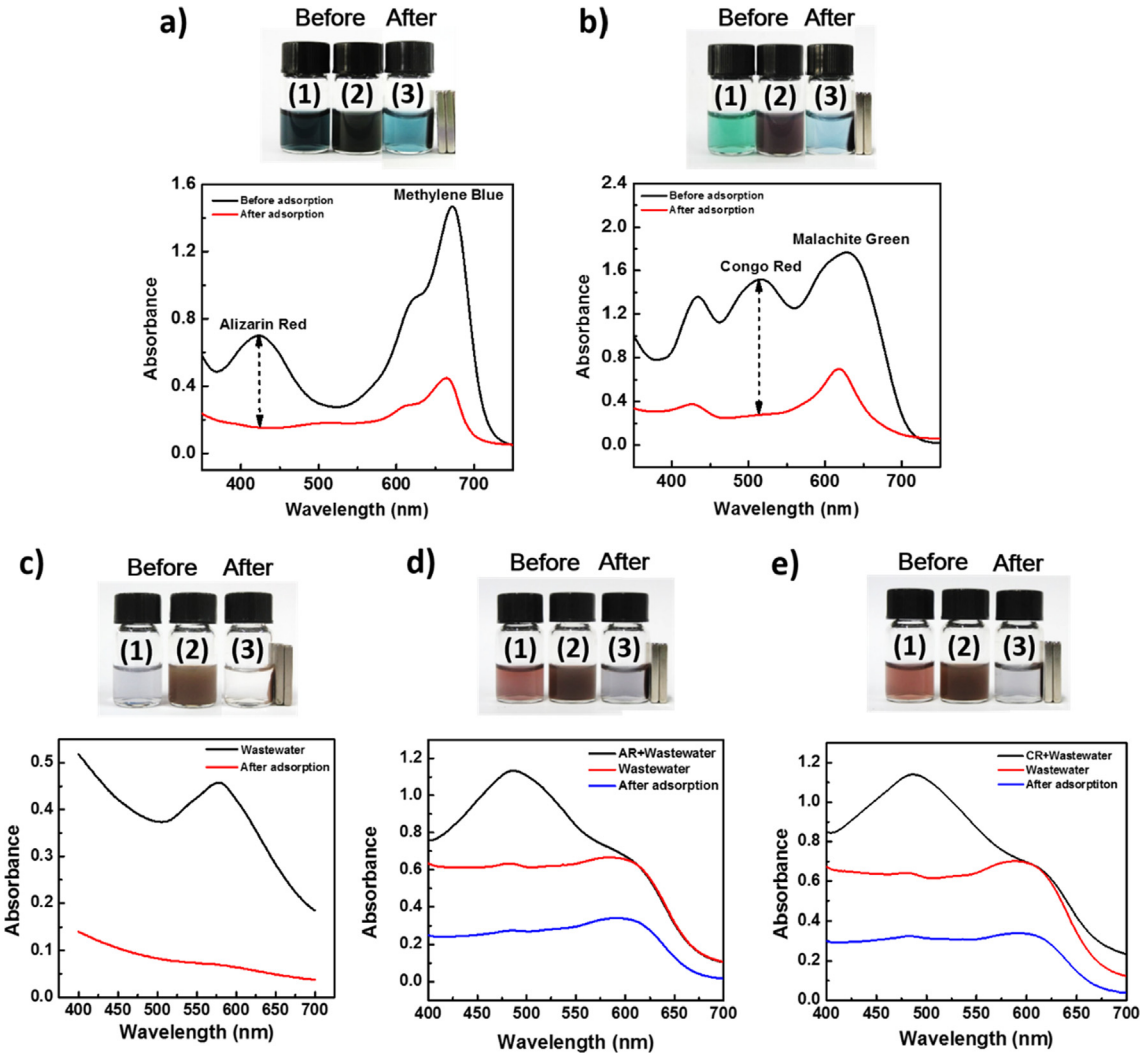

Fig. 10. Photographs (upper) and UV–vis spectra (lower) of mixed dye solution containing AR/MB (a) and CR/MG (b) before and after adsorption by Fe_3O_4@Tb/AMP core-shell nanoparticles. Photographs (upper) and UV–vis spectra (lower) of colored wastewater 1 from textile industry with anionic dye (c), colored wastewater 2 from textile industry with standard addition of AR (d) or CR (e) before and after adsorption by Fe_3O_4@Tb/AMP core-shell nanoparticles. Photographs: dye solution (1); dye solution with presence of adsorbents before (2) and after (3) magnetic separation.

Table 4
Adsorption efficiency of colored wastewater from textile industry calculated from Fig. 10.

Dye	Adsorption efficiency(%)
wastewater 1	99.31 ± 0.46
AR in wastewater 2	98.81 ± 2.15
CR in wastewater 2	99.53 ± 3.06

new avenue for cleanup of colored wastewater and probable industrial reuse of anionic dyes in future.

4. Conclusions

In this study, by fully exploring the adaptive nature of Tb/AMP infinite coordination polymer and rational design of the core-shell structure, novel magnetic Fe_3O_4@Tb/AMP core-shell nanoparticles with high magnetic susceptibility and selective adsorption for anionic dyes over cationic species were developed. Under the optimal condition, the maximum adsorption capacity calculated from Langmuir model of the Fe_3O_4@Tb/AMP core-shell nanoparticles was higher than most of adsorbents reported in the literature before and this nano-adsorbents could be easily recovered by an external magnet. All of these properties enabled anionic dyes being selectively removed from colored wastewater subsequently. The result of this study not only offered a clean and efficient water purification technology to eliminate of dye pollution in wastewater treatment purposefully, but also widen the application of infinite coordination polymer nanoparticles in environment field. Further work is in progress to develop novel technology of dye wastewater treatment with tailoring ICPs.

Acknowledgments

This research is financially supported by the National Natural Science Foundation of China (21505046 and 21675053), the China Postdoctoral Science Foundation (2016M590336 and 2017T100286) and the “Chenguang Program” funded by Shanghai Education Development Foundation and Shanghai Municipal Education Commission (15CG21).

References

[1] Y. Fan, H.-J. Liu, Y. Zhang, Y. Chen, Adsorption of anionic MO or cationic MB from MO/MB mixture using polyacrylonitrile fiber hydrothermally treated with hyperbranched polyethylenimine, J. Hazard. Mater. 283 (2015) 321–328.

[2] A. Bafana, S.S. Devi, T. Chakrabarti, Azo dyes: past, present and the future, Environ. Rev. 19 (2011) 350–371.
[3] W.X. Wang, G.H. Huang, C.J. An, X.Y. Xin, Y. Zhang, X. Liu, Transport behaviors of anionic azo dyes at interface between surfactant-modified flax shives and aqueous solution: Synchrotron infrared and adsorption studies, Appl. Surf. Sci. 405 (2017) 119–128.
[4] A. Banaei, S. Ebrahimi, H. Vojoudi, S. Karimi, A. Badiei, E. Pourbasheer, Adsorption equilibrium and thermodynamics of anionic reactive dyes from aqueous solutions by using a new modified silica gel with 2, 2'-(pentane-1, 5-diylbis (oxy)) dibenzaldehyde, Chem. Eng. Res. Des. 123 (2017) 50–62.
[5] G.Z. Kyzas, D.N. Bikiaris, N.K. Lazaridis, Selective separation of basic and reactive dyes by molecularly imprinted polymers (MIPs), Chem. Eng. J. 149 (2009) 263–272.
[6] G. Crini, P.-M. Badot, Application of chitosan, a natural aminopolysaccharide, for dye removal from aqueous solutions by adsorption processes using batch studies: a review of recent literature, Prog. Polym. Sci. 33 (2008) 399–447.
[7] G. Jethave, U. Fegade, S. Attarde, S. Ingle, Facile synthesis of Lead Doped Zinc-Aluminum Oxide Nanoparticles (LD-ZAO-NPs) for efficient adsorption of anionic dye: Kinetic, isotherm and thermodynamic behaviors, J. Ind. and Eng. Chem. 53 (2017) 294–306.
[8] C. Thamaraiselvan, M. Noel, Membrane processes for dye wastewater treatment: recent progress in fouling control, Crit. Rev. Env. Sci. Technol. 45 (2015) 1007–1040.
[9] C. Gadipelly, A. Pérez-González, G.D. Yadav, I. Ortiz, R. Ibáñez, V.K. Rathod, K.V. Marathe, Pharmaceutical industry wastewater: review of the technologies for water treatment and reuse, Ind. Eng. Chem. Res. 53 (2014) 11571–11592.
[10] Z. Hasan, S.H. Jhung, Removal of hazardous organics from water using metal-organic frameworks (MOFs): plausible mechanisms for selective adsorptions, J. Hazard. Mater. 283 (2015) 329–339.
[11] J.H. Qiu, Y. Feng, X.F. Zhang, M.M. Jia, J.F. Yao, Acid-promoted synthesis of UiO-66 for highly selective adsorption of anionic dyes: Adsorption performance and mechanisms, J. Colloid Interface Sci. 499 (2017) 151–158.
[12] J. Ma, F. Yu, L. Zhou, L. Jin, M.X. Yang, J.S. Luan, Y.H. Tang, H.B. Fan, Z.W. Yuan, J.H. Chen, Enhanced adsorptive removal of methyl orange and methylene blue from aqueous solution by alkali-activated multiwalled carbon nanotubes, ACS Appl. Mat. Interfaces 4 (2012) 5749–5760.
[13] B. Satilmis, P.M. Budd, Selective dye adsorption by chemically-modified and thermally-treated polymers of intrinsic microporosity, J. Colloid Interface Sci. 492 (2017) 81–91.
[14] D. Robati, B. Mirza, M. Rajabi, O. Moradi, I. Tyagi, S. Agarwal, V.K. Gupta, Removal of hazardous dyes-BR 12 and methyl orange using graphene oxide as an adsorbent from aqueous phase, Chem. Eng. J. 284 (2016) 687–697.
[15] X.Y. Wan, Y.Q. Zhan, Z.H. Long, G.Y. Zeng, Y. He, Core@double-shell structured magnetic halloysite nanotube nano-hybrid as efficient recyclable adsorbent for methylene blue removal, Chem. Eng. J. 330 (2017) 491–504.
[16] T.-S. Kim, H.J. Song, M.A. Dar, H.-J. Lee, D.-W. Kim, Fast adsorption kinetics of highly dispersed ultrafine nickel/carbon nanoparticles for organic dye removal, Appl. Surf. Sci. 439 (2018) 364–370.
[17] S. Saber-Samandari, S. Saber-Samandari, H. Joneidi-Yekta, M. Mohseni, Adsorption of anionic and cationic dyes from aqueous solution using gelatin-based magnetic nanocomposite beads comprising carboxylic acid functionalized carbon nanotube, Chem. Eng. J. 308 (2017) 1133–1144.
[18] H. Molavi, A. Hakimian, A. Shojaei, M. Raeiszadeh, Selective dye adsorption by highly water stable metal-organic framework: Long term stability analysis in aqueous media, Appl. Surf. Sci. 445 (2018) 424–436.
[19] J. Zhang, F. Li, Q. Sun, Rapid and selective adsorption of cationic dyes by a unique metal-organic framework with decorated pore surface, Appl. Surf. Sci. 440 (2018) 1219–1226.
[20] X.D. Du, C.C. Wang, J.G. Liu, X.D. Zhao, J. Zhong, Y.X. Li, J. Li, P. Wang, Extensive and selective adsorption of ZIF-67 towards organic dyes: Performance and mechanism, J. Colloid Interface Sci. 506 (2017) 437–441.
[21] P.C. Huang, F.Y. Wu, L.Q. Mao, Target-triggered switching on and off the luminescence of lanthanide coordination polymer nanoparticles for selective and sensitive sensing of copper ions in rat brain, Anal. Chem. 87 (2015) 6834–6841.
[22] Z.Z. Zhang, L. Wang, G.P. Li, B.X. Ye, Lanthanide coordination polymer nanoparticles as a turn-on fluorescence sensing platform for simultaneous detection of histidine and cysteine, Analyst 142 (2017) 1821–1826.
[23] M.D. Pluth, K.N. Raymond, Reversible guest exchange mechanisms in supramolecular host-guest assemblies, Chem. Soc. Rev. 36 (2007) 161–171.
[24] I. Imaz, J. Hernando, D. Ruiz-Molina, D. Maspoch, Metal-organic spheres as functional systems for guest encapsulation, Angew. Chem. Int. Ed. 48 (2009) 2325–2329.
[25] X.L. Zhang, J.J. Deng, Y.M. Xue, G.Y. Shi, T.S. Zhou, Stimulus response of Au-NPs@GMP-Tb core-shell nanoparticles: toward colorimetric and fluorescent dual-mode sensing of alkaline phosphatase activity in algal blooms of a freshwater lake, Environ. Sci. Technol. 50 (2016) 847–855.
[26] J.J. Deng, P. Yu, Y.X. Wang, L.Q. Mao, Real-time ratiometric fluorescent assay for alkaline phosphatase activity with stimulus responsive infinite coordination polymer nanoparticles, Anal. Chem. 87 (2015) 3080–3086.
[27] X.L. Zhang, J.J. Deng, G.Y. Shi, T.S. Zhou, Valence-tautomeric infinite coordination polymer nanoparticles for encapsulation of rhodamine B and its potential application for colorimetric and fluorescence dual mode sensing of hypochlorite, RSC Adv. 5 (2015) 107964–107969.
[28] P.C. Huang, J.J. Mao, L.F. Yang, P. Yu, L.Q. Mao, Bioelectrochemically active infinite coordination polymer nanoparticles: one-pot synthesis and biosensing property, Chem. Eur. J. 17 (2011) 11390–11393.
[29] R. Nishiyabu, N. Hashimoto, T. Cho, K. Watanabe, T. Yasunaga, A. Endo, K. Kaneko, T. Niidome, M. Murata, C. Adachi, Nanoparticles of adaptive supramolecular networks self-assembled from nucleotides and lanthanide ions, J. Am. Chem. Soc. 131 (2009) 2151–2158.
[30] F. Ding, W. Liu, J.-X. Diao, Y. Sun, Characterization of Alizarin Red S binding sites and structural changes on human serum albumin: a biophysical study, J. Hazard. Mater. 186 (2011) 352–359.
[31] A.K. Kondru, P. Kumar, S. Chand, Catalytic wet peroxide oxidation of azo dye (Congo red) using modified Y zeolite as catalyst, J. Hazard. Mater. 166 (2009) 342–347.
[32] R.S. Dariani, A. Esmaeili, A. Mortezaali, S. Dehghanpour, Photocatalytic reaction and degradation of methylene blue on TiO_2 nano-sized particles, Optik 127 (2016) 7143–7154.
[33] M. Khan, I.M.C. Lo, Removal of ionizable aromatic pollutants from contaminated water using nano γ-Fe_2O_3 based magnetic cationic hydrogel: Sorptive performance, magnetic separation and reusability, J. Hazard. Mater. 322 (2017) 195–204.
[34] M. Bahram, S. Asadi, G. Karimnezhad, Synthesized poly styrene-alt-maleic acid hydrogel for removal of azo dyes, methylene blue and methyl orange, from aqueous media, J. Iran. Chem. Soc. 12 (2015) 639–645.
[35] J.W. Fu, Z.H. Chen, M.H. Wang, S.J. Liu, J.H. Zhang, J.N. Zhang, R.P. Han, Q. Xu, Adsorption of methylene blue by a high-efficiency adsorbent (polydopamine microspheres): kinetics, isotherm, thermodynamics and mechanism analysis, Chem. Eng. J. 259 (2015) 53–61.
[36] Z.J. Du, Y. Zhang, Z.J. Li, H. Chen, Y. Wang, G.T. Wang, P. Zou, H.P. Chen, Y.S. Zhang, Facile one-pot fabrication of nano-Fe_3O_4/carboxyl-functionalized baker's yeast composites and their application in methylene blue dye adsorption, Appl. Surf. Sci. 392 (2017) 312–320.
[37] G.P. Li, L.Q. Mao, Magnetically separable Fe_3O_4-Ag_3PO_4 sub-micrometre composite: facile synthesis, high visible light-driven photocatalytic efficiency, and good recyclability, RSC Adv. 2 (2012) 5108–5111.
[38] H.Y. Niu, D. Zhang, Z.F. Meng, Y.Q. Cai, Fast defluorination and removal of norfloxacin by alginate/Fe@Fe_3O_4 core/shell structured nanoparticles, J. Hazard. Mater. 227–228 (2012) 195–203.
[39] Y.K. Long, L. Xiao, Q.H. Cao, Co-polymerization of catechol and polyethylenimine on magnetic nanoparticles for efficient selective removal of anionic dyes from water, Powder Technol. 310 (2017) 24–34.
[40] T. Moriguchi, K. Yano, S. Nakagawa, F. Kaji, Elucidation of adsorption mechanism of bone-staining agent alizarin red S on hydroxyapatite by FT-IR microspectroscopy, J. Colloid Interface Sci. 260 (2003) 19–25.
[41] Z.Y. Zhang, L. Moghaddam, I.M. O'Hara, W.O. Doherty, Congo Red adsorption by ball-milled sugarcane bagasse, Chem. Eng. J. 178 (2011) 122–128.
[42] B. Acemioğlu, Adsorption of Congo red from aqueous solution onto calcium-rich fly ash, J. Colloid Interface Sci. 274 (2004) 371–379.
[43] J.J. Deng, G.Y. Shi, T.S. Zhou, Colorimetric assay for on-the-spot alcoholic strength sensing in spirit samples based on dual-responsive lanthanide coordination polymer particles with ratiometric fluorescence, Anal. Chim. Acta. 942 (2016) 96–103.
[44] A.S. Patra, S. Ghorai, S. Ghosh, B. Mandal, S. Pal, Selective removal of toxic anionic dyes using a novel nanocomposite derived from cationically modified guar gum and silica nanoparticles, J. Hazard. Mater. 301 (2016) 127–136.
[45] H.Y. Zhu, R. Jiang, L. Xiao, Y.H. Chang, Y.J. Guan, X.D. Li, G.M. Zeng, Photocatalytic decolorization and degradation of Congo Red on innovative cross-linked chitosan/nano-CdS composite catalyst under visible light irradiation, J. Hazard. Mater. 169 (2009) 933–940.
[46] M. Ghaedi, A. Hassanzadeh, S.N. Kokhdan, Multiwalled carbon nanotubes as adsorbents for the kinetic and equilibrium study of the removal of alizarin red S and morin, J. Chem. Eng. Data. 56 (2011) 2511–2520.
[47] C. Gerente, V.K.C. Lee, P.L. Cloirec, G. McKay, Application of chitosan for the removal of metals from wastewaters by adsorption-mechanisms and models review, Crit. Rev. Env. Sci. Technol. 37 (2007) 41–127.
[48] P.Y. Wang, X.X. Wang, S.J. Yu, Y.D. Zou, J. Wang, Z.S. Chen, Silica coated Fe_3O_4 magnetic nanospheres for high removal of organic pollutants from wastewater, Chem. Eng. J. 306 (2016) 280–288.
[49] W. Plazinski, W. Rudzinski, A. Plazinska, Theoretical models of sorption kinetics including a surface reaction mechanism: a review, Adv. Colloid Interface Sci. 152 (2009) 2–13.
[50] F. Zhang, B.L. Ma, X.P. Jiang, Y.F. Ji, Dual function magnetic hydroxyapatite nanopowder for removal of malachite green and Congo red from aqueous solution, Powder Technol. 302 (2016) 207–214.
[51] M. Iram, C. Guo, Y. Guan, A. Ishfaq, H. Liu, Adsorption and magnetic removal of neutral red dye from aqueous solution using Fe_3O_4 hollow nanospheres, J. Hazard. Mater. 181 (2010) 1039–1050.
[52] S. Ghorai, A.K. Sarkar, A.B. Panda, S. Pal, Effective removal of Congo red dye from aqueous solution using modified xanthan gum/silica hybrid nanocomposite as adsorbent, Bioresour. Technol. 144 (2013) 485–491.
[53] L.Z. Bai, Z.P. Li, Y. Zhang, T. Wang, R.H. Lu, W.F. Zhou, H.X. Gao, S.B. Zhang, Synthesis of water-dispersible graphene-modified magnetic polypyrrole nanocomposite and its ability to efficiently adsorb methylene blue from aqueous solution, Chem. Eng. J. 279 (2015) 757–766.
[54] K.Y. Foo, B.H. Hameed, Insights into the modeling of adsorption isotherm systems, Chem. Eng. J. 156 (2010) 2–10.
[55] F. Pourebrahim, M. Ghaedi, K. Dashtian, F. Heidari, S. Kheirandish, Simultaneous removing of Pb^{2+} ions and alizarin red S dye after their complexation by ultrasonic waves coupled adsorption process: Spectrophotometry detection and optimization study, Ultrason. Sonochem. 35 (2017) 51–60.
[56] M. Fayazi, M. Ghanei-Motlagh, M.A. Taher, The adsorption of basic dye (Alizarin red S) from aqueous solution onto activated carbon/γ-Fe_2O_3 nano-composite:

kinetic and equilibrium studies, Mater. Sci. Semicond. Process. 40 (2015) 35–43.
[57] M.B. Gholivand, Y. Yamini, M. Dayeni, S. Seidi, E. Tahmasebi, Adsorptive removal of alizarin red-S and alizarin yellow GG from aqueous solutions using polypyrrole-coated magnetic nanoparticles, J. Environ. Chem. Eng. 3 (2015) 529–540.
[58] M. Roosta, M. Ghaedi, M. Mohammadi, Removal of Alizarin Red S by gold nanoparticles loaded on activated carbon combined with ultrasound device: Optimization by experimental design methodology, Powder Technol. 267 (2014) 134–144.
[59] D. Bharali, R.C. Deka, Adsorptive removal of congo red from aqueous solution by sonochemically synthesized NiAl layered double hydroxide, J. Environ. Chem. Eng. 5 (2017) 2056–2067.
[60] Y.J. Shao, B. Ren, H.M. Jiang, B.J. Zhou, L.P. Liping, J.Z. Ren, L.C. Dong, J. Li, Z.F. Liu, Dual-porosity Mn_2O_3 cubes for highly efficient dye adsorption, J. Hazard. Mater. 333 (2017) 222–231.
[61] C.S. Lei, M. Pi, C.J. Jiang, B. Cheng, J.G. Yu, Synthesis of hierarchical porous zinc oxide (ZnO) microspheres with highly efficient adsorption of Congo red, J. Colloid Interface Sci. 490 (2017) 242–251.
[62] H.T. Xie, X.P. Xiong, A porous molybdenum disulfide and reduced graphene oxide nanocomposite (MoS_2-rGO) with high adsorption capacity for fast and preferential adsorption towards Congo red, J. Environ. Chem. Eng. 5 (2017) 1150–1158.
[63] T. Wang, P. Zhao, N. Lu, H.C. Chen, C.L. Zhang, X.H. Hou, Facile fabrication of Fe_3O_4/MIL-101 (Cr) for effective removal of acid red 1 and orange G from aqueous solution, Chem. Eng. J. 295 (2016) 403–413.
[64] J. Abdi, M. Vossoughi, N.M. Mahmoodi, I. Alemzadeh, Synthesis of metal-organic framework hybrid nanocomposites based on GO and CNT with high adsorption capacity for dye removal, Chem. Eng. J. 326 (2017) 1145–1158.